Materials Science and Engineering B 113 (2004) 79–84

www.elsevier.com/locate/mseb

Fabrication and characterization of low temperature (<450 °C) grown p-Ge/n-Si photodetectors for silicon based photonics

P.R. Bandaru[a,*], S. Sahni[a], E. Yablonovitch[a], J. Liu[b], H.-Jun Kim[b], Y.-H. Xie[b]

[a] *Department of Electrical Engineering, University of California at Los Angeles, Los Angeles, CA 90095, USA*
[b] *Department of Materials Science and Engineering, University of California at Los Angeles, Los Angeles, CA 90095, USA*

Received 23 March 2004; accepted 3 July 2004

Abstract

P–n hetero-junctions were fabricated by depositing p-Ge thin films on n-Si substrates using molecular beam epitaxy and electron-beam evaporation, with processing temperatures less than 450 °C, to be compatible with back-end silicon processing. The surface preparation of the Si substrate prior to Ge deposition was found to significantly affect the crystallinity of the deposited Ge layers and, hence, the p–n photodetector diode characteristics. The quality of the deposited Ge layers was inferred both through electrical and optical measurements as well as through structural characterization, i.e. X-ray diffraction (XRD). Surface desorption treatments to remove adsorbed hydrogen, oxygen and hydrocarbons were attempted to improve the Si surface quality to increase the minority carrier diffusion lengths and minimize dark current densities. Hydrogen desorption treatment at 450 °C prior to Ge deposition gave the best performance with diffusion lengths greater than 25 nm and dark currents of 0.3 mA/cm^2. The observed performance from the p–n diodes is expected to be sufficient for fabricating waveguide integrated photodetectors with high responsivities.

Keywords: Germanium; Silicon; p-n junctions; Semiconductor devices; Silicon based photonics; Photodetector

1. Introduction

As micro-electronic systems continue to scale down, the resultant increased electrical interconnect density gives rise to both increased power dissipation and a reduced speed of operation due to cross-talk [1]. One approach to mitigate both of the above problems is to use optical interconnects and systems. The use of silicon (Si) and Si compatible materials and systems is desirable for the optical components, as this would make use of the existing micro-electronics industry infrastructure based on complementary metal-oxide-semiconductor (CMOS) technology. We address in this paper, the development of novel low temperature (<450 °C) thin film deposition processes using electron-beam evaporation and molecular beam epitaxy, for the fabrication of p-Ge/n-Si photodetectors. These processes, and the understanding gained, can be used for photonic devices that can be seamlessly integrated with existing CMOS based electronics.

The detection of light in a Si based setting is a very challenging problem. In the wavelength range used in fiber-optic communication systems (1.3–1.55 μm), InP based direct band-gap semiconductors have very high efficiency and speed of operation. However, the integration of InP with Si electronics is quite difficult [2]. One possible solution is to use germanium (Ge), which has a high absorption coefficient in the wavelength range of 1.3–1.55 μm [3] and can function well as a photodetector. However, the lattice parameter mismatch between Ge and Si (4.2%) and the high temperatures (650–800 °C) needed for Ge on Si growth and cleaning [4] are two obstacles that have to be overcome prior to reliable photodetector fabrication.

* Corresponding author. Present address: Department of Mechanical and Aerospace Engineering, University of California, 9500 Gilman Drive, Mail Code 0411, La Jolla, San Diego, CA 920930411, USA. Tel.: +1 858 5345325; fax: +1 858 5345698.
E-mail address: pbandaru@ucsd.edu (P.R. Bandaru).

0921-5107/$ – see front matter © 2004 Elsevier B.V. All rights reserved.
doi:10.1016/j.mseb.2004.07.007

In this paper, we report the results of a study conducted to probe the performance of photodetectors fabricated by depositing Ge thin films on Si substrates at temperatures low enough (<450 °C) to be compatible with back-end CMOS processing. While the photo-response of the fabricated devices would not be expected to be comparable to the high-temperature processed devices, the aim was to see whether it would be adequate for efficient back-end CMOS integration. A back-end integration route (fabricating photonic devices on top of existing CMOS based electronics) is advocated as it avoids changes in standard foundry practices leading to easier adoption and widespread use of Si based photonics devices. However, the major constraint is that the temperature in back-end processing is usually restricted to less than 450 °C to avoid damage or degradation to the Al/Ti based micro-electronic component interconnects.

It has been shown previously that electron-beam evaporation of polycrystalline Ge on Si substrates [5] at 300 °C yields photodetectors with moderate performance (<20 mA/W responsivity and >1 mA/cm^2 dark current densities). We attempt here to improve upon and extend the above work using both electron-beam evaporation (e-beam) and molecular beam epitaxy (MBE), confronting fundamental barriers to performance involving deposition rate, temperature and prior Si substrate surface preparation. To the investigators' knowledge, this is the first time that MBE has been used for low-temperature Ge deposition, for use in photodetectors. As MBE is carried out at much lower background pressures (10^{-8} Pa vis-à-vis e-beam evaporation at 10^{-6} Pa), lower impurity incorporation and better quality Ge films are expected.

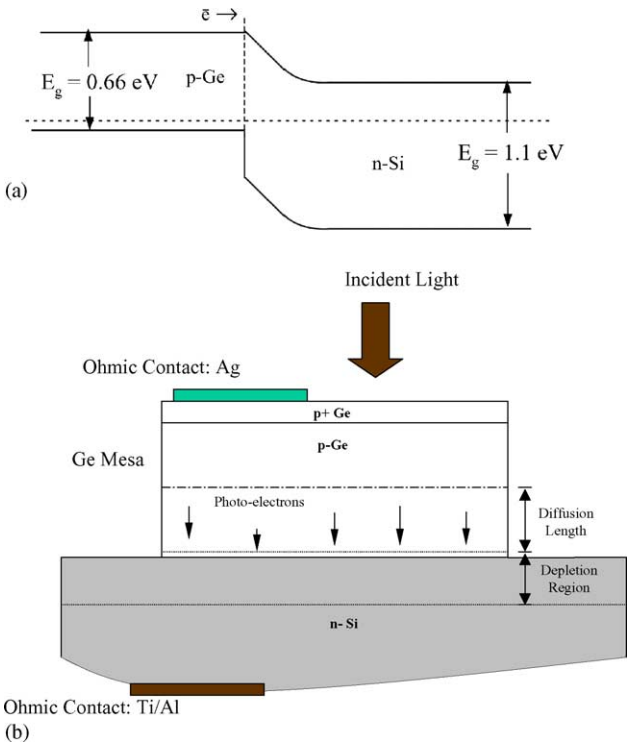

Fig. 1. (a) p-Ge/n-Si band alignment, consistent with the experimental results presented in this paper. The depletion region is shown to be completely on the silicon side of the junction. (b) Schematic diagram of the thin film structure. The photo-electrons, responsible for the photo-response, diffuse towards the depletion region.

2. Using the minority carrier diffusion length (L_n) to characterize deposited p-Ge films

In our experiments, we fabricate p-Ge/n-Si photodiodes, by depositing p-Ge thin films on n-Si substrates, and the measured photo-response gives us an indication of the quality of the deposited Ge layer. The band structure and physical layout of the fabricated photodetector is shown in Fig. 1. The doping level in as-deposited p-Ge (p: 10^{17} cm^{-3}) is much higher than in the substrate (n: 10^{15} cm^{-3}); the depletion region is almost completely [3,6] in the Si. As a result, the photo-response of the p–n junction is mainly derived from the diffusion of photo-carriers into the depletion region and subsequent collection.

Since the aim of this paper is to characterize the Ge film growth, we quote the results of our photo-response measurements in terms of electron (minority carriers in p-Ge) diffusion length in the Ge (L_n) and not responsivity as is conventional. Responsivity (R) is not as fundamental as L_n; it is wavelength dependent and varies with specific layer and device design, e.g., R can be enhanced by the use of anti-reflecting films. In another example, which will be described in detail later, integrated waveguide photodetectors could be used to achieve high photo-response using the high refractive index contrast silicon-on-insulator (SOI) material system. A large diffusion length (L_n) would translate to an intrinsically large photo-response.

The diffusion length (L_n) is estimated from the normal incidence responsivity values (in mA/W) using an absorption co-efficient, α of 10^4 cm^{-1} (at 1.31 μm) [3].

3. Experimental procedure

We fabricate p–n junction photodetectors by depositing 200 nm thick p-Ge thin-films (B doped) on n-Si (1 0 0) substrates (ρ: 2–6 Ω cm) both by e-beam evaporation (CHA: base pressure of $4{\cdot}10^{-4}$ Pa; temperature = 300 ± 10 °C, and MBE (Riber EVA 32: base pressure 8×10^{-7} Pa; temperature = 370 ± 25 °C). In the MBE samples, the top 10 nm of the Ge was doped p$^+$ to reduce the metal–Ge contact resistance (Fig. 1(b)). Prior to Ge deposition, the Si substrates were cleaned successively for 2 min each in de-ionized water, acetone, *iso*-propanol and Piranha reagent ($H_2O_2 + H_2SO_4$). The samples were then treated with a final dip in buffered HF, which passivates the Si and leads to a surface stable in air [7].

The surface preparation of the Silicon was found to be critical in determining the magnitude and nature of the photo-response and electrical leakage. When the Si (1 0 0) sub-

Table 1
Processing conditions for the MBE grown (M) Ge films

Surface preparation surface of Si substrate	Growth rate (Å/s)		
	2.5	1.0	0.2
Only HF clean	Sample M4	Sample M1	Sample M5
HF clean + 450 °C hydrogen desorption (15 min)			Sample M7
HF clean + 200 °C hydrocarbon desorption (50 min)			Sample M9
HF clean + 200 °C hydrocarbon desorption (50 min) + 450 °C hydrogen desorption (15 min)			Sample M12
Piranha clean + 800 °C oxide desorption			Control sample M3

The Ge deposition in all the samples was done by MBE at 370 °C (the samples are numbered in the order in which they were grown).

strate is treated with HF, the surface is completely terminated with H atoms, which could hinder the proper registration of Ge adatoms with the Si substrate. Ambient hydrocarbon and oxide contamination also contributes to degrading the Si surface. With these issues in mind, we attempted to remove the H atoms in situ by a pre-deposition heating treatment at 450 °C in a few samples (see Table 1). To desorb the hydrocarbons from the surface, a 200 °C pre-bake for 50 min [8], was done in some samples. Additionally, a control sample, M3 in Table 1, was fabricated where an oxide terminated Si substrate was subjected to the standard 800 °C oxide desorption anneal before Ge film deposition [4].

During MBE growth, the deposition of Ge on Si was monitored by reflection high energy electron diffraction (RHEED). The overall crystal quality and strain of the as-grown Ge/Si structures was analyzed by ex situ X-ray diffraction (θ–2θ and rocking curve analysis), using the Cu $K\alpha_1$ (1.5406 Å) line, in a Bede3 diffractometer. An atomic force microscope (AFM) was used to characterize the surface roughness, found to be $\sim 1.5 \pm 0.4$ nm in all the samples.

The electrical properties of both (a) large (5 mm × 5 mm) and (b) 400 μm × 400 μm Ge mesa–Si p–n junctions were studied. Ge mesa etching was done by a HF:H_2O_2:acetic acid (1:2:20) mixture. Ohmic contacts were made to the n-silicon and p-germanium by e-beam evaporation at room temperature. Depositing Ti (15 nm)/Al (200 nm) on n-Si and Ag (300 nm) on p-Ge, gives the lowest contact resistance.

The sample was illuminated by 1310 nm light (using a Thor labs mid-IR single mode laser diode), from the Ge side (no difference was observed when light is shone from the bottom Si side) in the 0–3 mW range. The responsivity was measured on a reverse biased p–n junction, using both dc and ac lock-in methods. In the ac technique, the laser diode light was modulated by an optical chopper and the photo-response voltage read by a lock-in amplifier.

4. Results and discussion

4.1. Thin film growth

In RHEED, initially the hydrogenated Si (1 0 0) surface was observed to be (1 × 1) reconstructed [9] at the growth temperature of 370 °C (for the control sample, a (2 × 1) pattern is seen at 800 °C due to an oxide desorbed, cleaner Si surface). The RHEED pattern gradually changes from (1 × 1) to (2 × 1), after about 70 nm of Ge have been deposited. Fig. 2 shows a typical (2 × 1) RHEED pattern taken *after* the completion of the Ge deposition. At low growth temperatures (<400 °C), the diffusion of Ge adatoms is severely hindered precluding the formation of a Ge wetting layer and idealized Stranski–Krastanov growth [10]. Subsequent Ge film deposition diminishes the effect of the initial surface roughness; the misfit strain in the film has also been accommodated by now through the formation of strain relieving defects. The above facilitate Ge diffusion and the (2 × 1) reconstruction of the surface.

The results of ex situ X-ray diffraction (XRD) are shown in Fig. 3. The θ–2θ curve for a typical MBE grown Ge film (sample M9 in Table 1) indicates, as shown in Fig. 3(a), that the Ge layer is almost completely relaxed. Fig. 3(b) gives a comparison of the rocking curves for samples grown by MBE (sample M9) and e-beam evaporation (sample E3: Table 2). As the width of the rocking curve is inversely proportional to the crystalline quality of the deposited film, it is inferred from Fig. 3(b) that the MBE films are superior to the e-beam evaporated films, as expected.

4.2. Electrical properties

4.2.1. Diffusion length and leakage current

Fig. 4(a) and (b) give the minority carrier diffusion lengths (L_n) measured for samples processed under different conditions. It is seen from Fig. 4(a) that L_n strongly varies with the Si surface preparation. Although hydrocarbon desorption

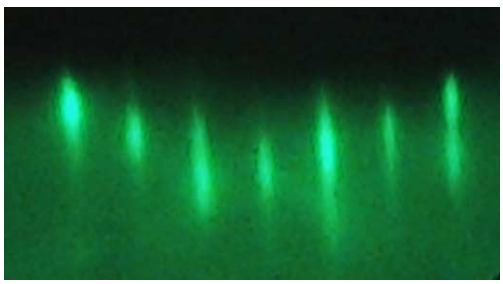

Fig. 2. A typical (2 × 1) RHEED pattern after the completion of the Ge growth at 370 °C, indicating the formation of a single crystal film.

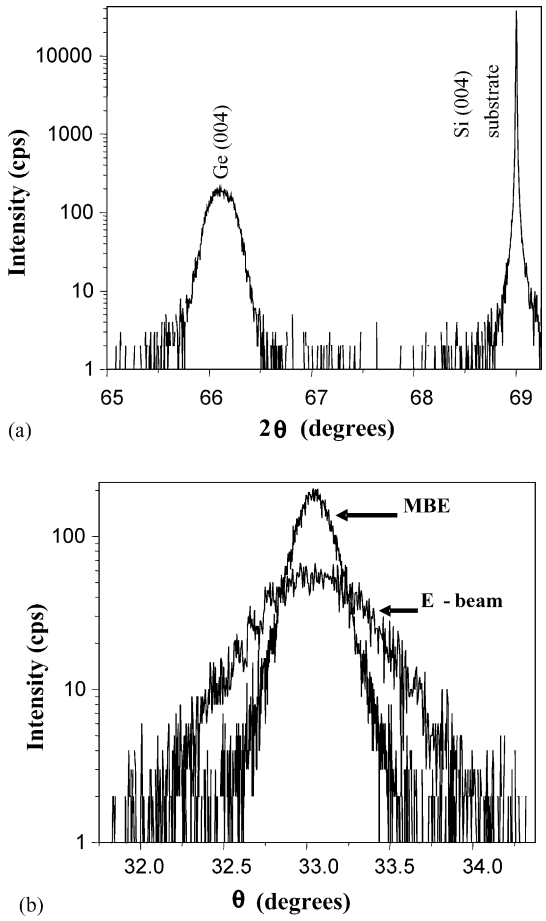

Fig. 3. (a) A typical θ–2θ X-ray diffraction spectrum of the p-Ge/n-Si photodetector (sample M9). The (0 0 4) peaks for the Si substrate and for the Ge epi-layer are shown. (b) A comparison of the X-ray rocking curves of typical MBE (sample M9) and e-beam grown (sample E3) p-Ge films on a Si substrate. The full width at half maxima (FWHM) is ∼0.3° in the MBE sample, and ∼0.7° in the e-beam sample.

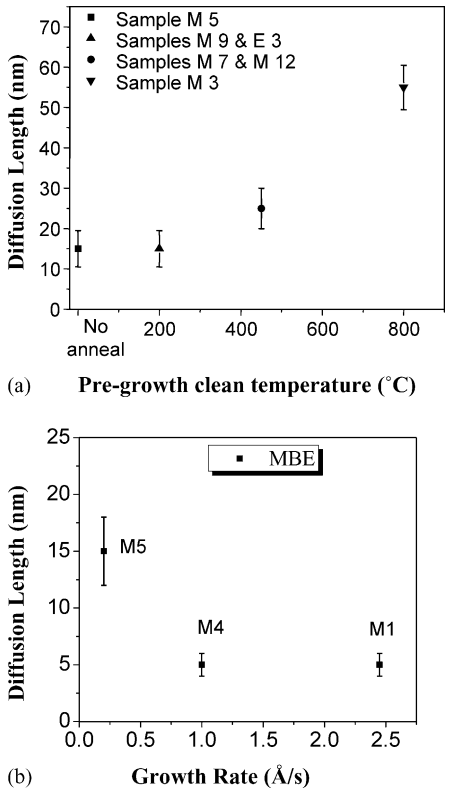

Fig. 4. (a) The variation of the diffusion length (L_n) as a function of pre-deposition surface cleaning temperatures (Table 1 lists the exact growth process for the samples). (b) The variation of the diffusion length (L_n) as a function of growth rate. The experimental points represent samples grown by MBE at 370 °C with no prior annealing (samples M1, M4 and M5; see Table 1).

seems to be ineffective in enhancing the L_n in the present study, the hydrogen and oxide desorption steps do seem to improve the deposited Ge film quality. The hydrogen desorption anneal at 450 °C improves the value of L_n (samples M5 versus M7). The control sample (M3), processed with an oxide clean at 800 °C, has an L_n of ∼60 nm. It is then seen that the performance of our low temperature processed devices is off by only a factor of 2, and can be further improved by more careful surface cleaning procedures.

The temperature ceiling for the hydrogen removal was set at 450 °C, due to the limitations of back-end CMOS processing. Since complete H desorption occurs only at temperatures exceeding 600 °C [11], a lower temperature treatment implies that the Si surface was not completely devoid of hydrogen. Our results on the e-beam evaporated Ge samples (e.g. sample E3), gave results similar to those reported by Masini *et al.*, [5]. Fig. 5 shows the dependence of the diffusion length of carriers in the Ge on growth rate, which illustrates that the quality of the epitaxial layer improves at lower growth rates.

The dc current–voltage characteristics of a typical MBE grown p-Ge/n-Si photodiode (sample M7) are shown in Fig. 5. The leakage current in all the MBE samples was in the range of 0.2–0.3 mA/cm^2 at −1 V reverse bias, which is the *lowest reported* for Ge–Si photodetectors [12]. The electron-beam evaporated samples (samples E1 and E3 in

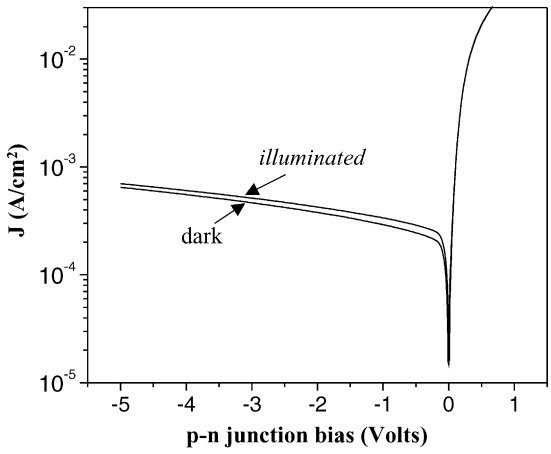

Fig. 5. Current density (J)–voltage (V) curves for the p-Ge/n-Si photodiodes, with (*illuminated*) and without (*dark*) light.

Table 2
Processing conditions for the electron-beam evaporated (E) Ge films

Surface preparation of Si substrate	Growth rate (Å/s)	
	1.5	0.5
Only HF clean	Sample E1	
HF clean + 200 °C hydrocarbon desorption (50 min)		Sample E3

The growth temperature was 300 °C (the samples are numbered in the order in which they were grown).

Table 2), on the other hand, give higher leakage currents of about 1.6–1.8 mA/cm^2.

4.2.2. Modeling the leakage current

The leakage under reverse bias was modeled by considering the two components of the reverse current [13] viz.: (1) leakage current from defects at the p–n junction interface, the *generation current*, and (2) a *diffusion current* component arising from outside the space charge region in the Ge. Since the depletion region resides almost completely in the Si, the generation current within the space charge region including the Ge is neglected.

4.2.2.1. Generation current. The leakage current density from the Ge–Si interface, J_{gen}, can be estimated as

$$J_{gen} \approx e n_{Ge} v_s \quad (1)$$

Here, n_{Ge} is the minority carrier concentration in the Ge and v_s is the surface recombination velocity. n_{Ge} in our devices is $\sim 10^9$ cm^{-3} ($n_{Ge} = n_i^2/p$). To estimate the maximum possible leakage current, we assume a reasonably high value of v_s (10^6 cm/s), typical for a defective semiconductor surface [3,13,14]. Using these values, J_{gen} is calculated to be $\sim$0.15 mA/cm^2.

4.2.2.2. Diffusion current. This component of the leakage current density arises from outside the depletion region. Minority carriers (electrons in p-Ge and holes in n-Si) diffuse to the edge of the space charge region and are then swept by the reverse bias to the Ohmic contacts. Since the minority carrier concentration in the p-Ge is much higher than in the n-Si (by a factor of about 10^4), we only consider the diffusion leakage current on the Ge side. The diffusion component ($J_{diff,n}$) of the leakage current density in the p-Ge is

$$J_{diff,n} \approx q \frac{n_{Ge}}{\tau_n} L_n \quad (2)$$

Here, τ_n is the minority carrier lifetime in the p-Ge. τ_n is estimated to be $\sim$2.5 ps from the diffusion coefficient (D_n) and L_n [3]. We measured, using the hall effect, a value of mobility (μ_n) of p-Ge of $\sim$100 cm^2/V s, in the MBE samples. Using these values in Eq. (2) we calculate $J_{diff,n} \sim$0.15 mA/cm^2.

Combining $J_{diff,n}$ and J_{int}, the total reverse leakage current density is $\sim$0.3 mA/cm^2, which agrees quite well with the experimental values of 0.2–0.3 mA/cm^2 in the MBE samples. However, these models predict the leakage in the e-beam samples to be of the same order due to the similar values of L_n, while the observed leakage is $\sim$1.7 mA/cm^2. The poorer crystalline quality of the Ge in the e-beam samples (evidenced through X-ray diffraction), probably results in a lower electron mobility and higher surface recombination velocity increasing the leakage current density.

In analyzing the reverse leakage currents it is worth noting that, for the case of p-Ge, the diffusion of electrons towards the depletion region could be impeded by an energy barrier due to the large number of dislocations, which act as acceptor sites for electrons, at the Ge/Si interface [15]. The presence of a barrier is suggested in some samples where high photoresponse is accompanied by a correspondingly high reverse leakage current density. However, these effects are not very significant and the departure from typical values of leakage current densities is quite small. So, even though the assumption of an energy barrier at the Ge/Si interface would make the leakage model more complete, we do not include the barrier in our analysis because its impact on the overall performance trends in our devices is negligible.

4.3. Dependence of photo-response on wavelength and input power

It is seen (Fig. 6) that the photo-current scales linearly with the incident laser power in all the devices (i.e. the responsivity stays constant), indicating stable operation over a wide range of input power.

The spectral variation of the absorption coefficient of the epitaxial Ge films (Fig. 7) follows closely that of bulk single crystal Ge in the optical communications window of 1.3–1.55 μm, proving the feasibility of use of the fabricated p-Ge/n-Si photodetectors in an integrated environment. Although the MBE deposited Ge is single crystalline, it is still expected to be heavily defective due to the low growth temperature and the lattice mismatch with the Si substrate. The imperfect film is probably responsible for the lack of a sharp transition at 1.55 μm.

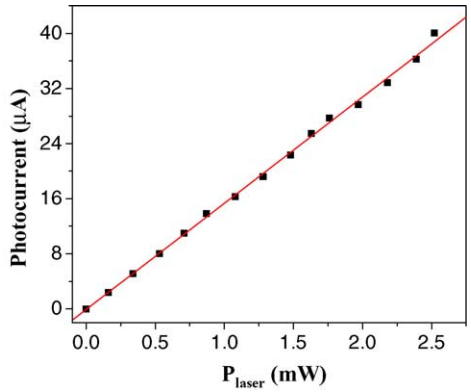

Fig. 6. The photo-current of the p-Ge/n-Si photodiodes scales linearly with incident laser power. We show the variation for MBE sample M7, reverse biased, at −3 V.

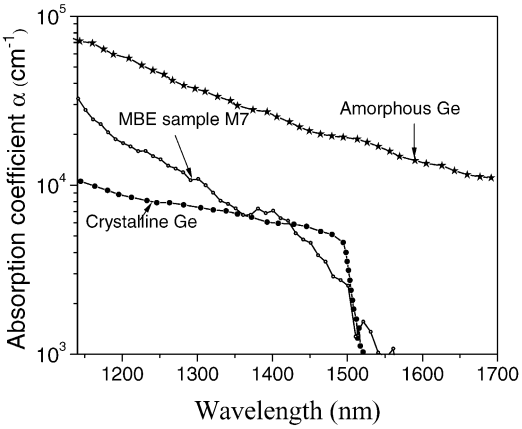

Fig. 7. The spectral variation of absorption coefficient measured for sample M7 contrasted with the curves for single-crystal and amorphous Ge [5].

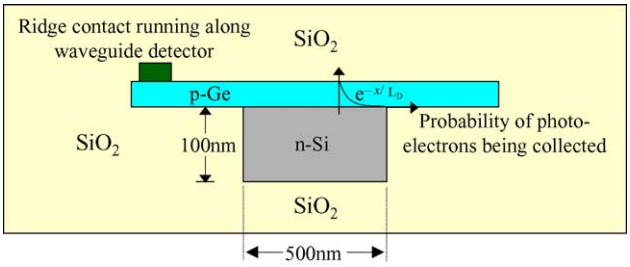

Fig. 8. Cross-section of a proposed waveguide photodetector based on the Ge/SOI system. The high index contrast provided by an SOI wafer is ideal for this application. The thickness of the silicon layer is designed for a single mode waveguide.

4.4. Preferred device design: waveguide integrated photodetectors

As outlined earlier in Section 2, photonics in a high refractive index contrast system (e.g. using a SOI substrate), would be implemented by integrating a photodetector with a waveguide. Fig. 8 shows the cross-sectional view of one such implementation. If the thickness of the Ge is limited to one diffusion length (L_n), then all the photo-carriers generated by the light propagating in the waveguide would be collected by diffusion and very high photo-response can be expected. A thicker Ge layer, with a correspondingly larger L_n, would increase overall efficiency of the Ge photodetector by ensuring that most of the waveguide mode is transferred to the Ge. The results presented in this paper indicate that the Ge need not be made very thin as simple fabrication techniques compatible with back-end CMOS processing can give reasonable values of diffusion lengths in Ge.

5. Conclusions

We have explored the feasibility of a p-Ge/n-Si photodetector for Silicon based photonics applications, fabricated by low temperature molecular beam epitaxy and e-beam evaporation, compatible with back-end CMOS processing. It was seen that the substrate surface preparation, processing conditions and growth temperature are critical in determining the crystalline quality of the grown Ge films, and consequently the diffusion length of the minority carriers and overall photodetector performance. By modifying the deposition rate and adopting various Si surface cleaning methods for the removal of hydrogen and ambient contamination, we have obtained minority carrier diffusion lengths (L_n) and photo-response adequate for waveguide-integrated photodetectors. The measured leakage current densities in our p-Ge/n-Si photodiodes are among the lowest reported. The leakage currents were modeled by conventional mechanisms of space charge generation and carrier diffusion, with the carrier lifetime being limited by interface defects and dislocation induced recombination centers. It remains to be seen whether the advantages conferred by low temperature processing vis-à-vis device performance can be utilized in a practical electronics integrated photonic device platform.

Acknowledgments

We gratefully acknowledge the help of Atif Noori in the X-ray diffraction of the samples, and Ivan Alvarado in the measurement of the spectral variation of the responsivity. The authors would also like to acknowledge the use of the nano-electronics laboratory facility at UCLA. This work was supported in part by Defense Advanced Research Projects Agency, MDA972-02-1-0019. The content of the information does not necessarily reflect the position or the policy of the government and no official endorsement should be inferred.

References

[1] E.A. Fitzgerald, L.C. Kimmerling, MRS Bull. 23 (4) (1998) 39.
[2] A. Bandyopadhyay, M.J. Deen, in: H.S. Nalwa (Ed.), Photodetectors and Fiber Optics, Academic Press, New York, 2001 (Chapter 5).
[3] S.M. Sze, Physics of Semiconductor Devices, 2nd ed., Wiley, New York, 1999.
[4] G.P. Watson, E.A. Fitzgerald, Y.H. Xie, D. Monroe, J. Appl. Phys. 75 (1994) 263.
[5] G. Masini, L. Colace, F. Galluzzi, G. Assanto, Mater. Sci. Eng. B 69/70 (2000) 257.
[6] H-C. Luan, K. Wada, L.C. Kimmerling, G. Masini, L. Colace, G. Assanto, Opt. Mater. 17 (2001) 71.
[7] G.W. Trucks, K. Raghavachari, G.S. Higashi, Y.J. Chabal, Phys. Rev. Lett. 65 (1990) 504.
[8] D.J. Eaglesham, G.S. Higashi, M. Cerullo, Appl. Phys. Lett. 59 (1991) 685.
[9] J. Ihm, M.L. Cohen, D.J. Chadi, Phys. Rev. B 21 (1980) 4592.
[10] M. Ohring, The Materials Science of Thin Films, Academic Press, San Diego, 2002.
[11] V. Le Thanh, Thin Solid Film 321 (1998) 98.
[12] L. Colace, G. Masini, G. Assanto, IEEE J. Quant. Elec. 35 (1999) 1843.
[13] A.S. Grove, Physics and Technology of Semiconductor Devices, Wiley, New York, 1967.
[14] E. Yablonovitch, R. Bhat, C.E. Zah, T.J. Gmitter, M.A. Koza, Appl. Phys. Lett. 60 (1992) 371.
[15] G. Masini, L. Colace, G. Assanto, H.-C. Luan, L.C. Kimerling, IEEE Trans. Elect. Devices 48 (6) (200) 11092.